Soft Matter

PAPER

View Article Online
View Journal

Cite this: DOI: 10.1039/d0sm01641a

Synergistic effect of hydrophobic and hydrogen bonding interaction-driven viologen–pyranine charge-transfer aggregates: adenosine monophosphate recognition†

Redhills L. Narendran and Archita Patnaik *

Understanding the role of non-covalent interactions that dictate and fine-tune the direction of self-assembly of functional molecules is crucial for developing stimuli responsive materials. Herein, we systematically designed and synthesized viologen derivatives with hydrophobic dodecyl chains and alkyl carboxylic acid functionalities. The complementary electronic and electrostatic counterpart of viologens was chosen as pyranine. Viologens comprising of a hydrophobic dodecyl chain on one terminal and hydrogen bonding alkyl carboxylic acid on the other (**V1** and **V2**) underwent aggregation to a varying extent upon interaction with pyranine. The length of the alkyl carboxylic acid had a greater impact on the nature and morphology of the aggregates. Control molecules (**V3** and **V4**) in which 4,4′-bipyridine was symmetrically quaternized with alkyl carboxylic acids did not aggregate upon interaction with pyranine. The delicate balance existing between the hydrophobicity of the dodecyl chains and the intermolecular hydrogen bonding interaction between the alkyl carboxylic acid groups in **V1** or **V2** of the corresponding charge transfer (CT) complexes was instrumental in driving the aggregation. The CT aggregates of [**V1**–Pyr] and [**V2**–Pyr] exhibited excellent stability in water which disaggregated at physiological pH. We emphasize on the importance of synergy between hydrophobic and hydrogen bonding interactions in reinforcing each other to drive the supramolecular aggregation of the CT complexes. Such pH dependent CT aggregates are of importance as scaffolds in pH controlled drug release. In the present study, the CT aggregates were evaluated for adenosine nucleotide recognition in water; [**V1**–Pyr] and [**V2**–Pyr] exhibited selective response towards adenosine monophosphate *via* deprotonation induced dissolution of aggregates in water leading to emission enhancement.

Received 12th September 2020,
Accepted 17th November 2020

DOI: 10.1039/d0sm01641a

rsc.li/soft-matter-journal

Introduction

Self-assembly of functional molecules giving rise to diverse supramolecular architectures is dictated by intermolecular forces of varying nature such as van der Waals interactions, π–π stacking, hydrogen bonding, hydrophobic interactions, charge-transfer (CT) interactions, metal–ligand binding and electrostatic interactions.[1] Tinkering with the nature of functional groups on molecular systems enables facile construction of geometry-specific self-assembled structures and endows them with superior functionality.[2] CT complexes are formed from the association of electron rich and electron deficient molecules in which a portion of electronic charge is transferred from the donor to acceptor.[3,4] Among the non-covalent interactions, CT interactions are key candidates towards engineering functional molecular ensembles and nanostructures from molecules with complementary electronic nature leading to molecular systems with enhanced multitude of functionalities.[5] Catenanes, rotaxanes, pseudo-rotaxanes, molecular shuttles, molecular motors, molecular tweezers and clips, foldamers, gels, liquid crystals, *etc.*, were developed with their roots centred on CT interactions.[6–11] Self-assembly driven by CT interactions between molecules and generation of micro- and nano structures differing from their congeners arouse curiosity with regard to the rationale behind the emergence of such structures.[12] The strength of such molecular assemblies increases when one type of non-covalent interaction reinforces the other and *vice versa*, leading to substantial changes in their morphology and physicochemical properties.

Aggregation of amphiphiles in water drives the formation of micelles, vesicles and a large variety of nano and microscale aggregates depending on the concentration and structure of the amphiphile.[13] The nature of the aggregates formed and the

Colloids and Interfaces Laboratory, Department of Chemistry, Indian Institute of Technology Madras, Chennai, India. E-mail: archita@iitm.ac.in

† Electronic supplementary information (ESI) available. See DOI: 10.1039/d0sm01641a

resultant properties are controlled by the trade-off between hydrophobic and hydrophilic moieties in the amphiphile.[14] The length of alkyl chains, branching in alkyl chains, counter ions, charge on the head group, functional groups and stimuli responsive moieties in the amphiphile influence the morphology and function of aggregates.[15–17] Introduction of a CT responsive moiety into the structure of an amphiphile which is susceptible to interaction with its electrostatic counterpart enhances the scope of fine-tuning the aggregate morphology.[18] Such CT responsive amphiphiles could find their utility in developing stimuli responsive molecular systems and in fabricating materials for opto-electronic applications.

Viologens are dicationic organic salts with versatile physicochemical properties. They exhibit multiple redox states in response to appropriate stimuli.[19,20] By virtue of their highly electron deficient nature, viologens are susceptible to CT interactions with electron rich molecules. They form CT complexes with derivatives of dihydroxy naphthalene, sulfonated pyrene, tetrathiafulvalene, tetraphenylborate, ferrocyanide, indole derivatives, carboxylates, *etc.* upon encashing on the complementary electronic or electrostatic nature of these molecules.[21–28] The dicationic nature of viologens facilitates their interaction with biologically relevant nucleotides to polyelectrolytes of biological importance, such as ss and ds DNA.[29,30] de Borba *et al.*[31] were the first to report that paraquat and pyranine form CT complexes in aqueous solution. Pyranine (8-hydroxypyrene-1,3,6-trisulfonic acid trisodium salt) is a negatively charged, water soluble fluorophore and a photoacid. Viologen–pyranine CT complexes were used to develop indicator displacement assay based sensors towards monosaccharides, α-hydroxy carboxylates, nucleotides, *etc.*, where the emission of pyranine was used as a marker to quantify the corresponding analytes.[32–35] CT interactions between amphiphilic viologen derivatives and pyranine were used to facilitate morphological transitions from 2D nanosheets to 1D nanofibers[36,37] and from vesicles to sheets,[38] generation of ultralong nanofibers with tuneable straightness[39] and formation of redox responsive hydrogels.[40] Generation of such nanostructures and realization of morphological transitions in the above mentioned viologen–pyranine complexes were mainly attributed to the combination of CT, electrostatic, π–π stacking and hydrophobic interactions, devoid of hydrogen bonding.

Hydrogen bonding is ubiquitous in nature and its importance in maintenance and functioning of biological systems is a topic of intense study spanning across the realms of science.[41] Developing materials with propensity to interact with their surroundings *via* hydrogen bonds generated new directions towards the development of robust molecular materials.[42,43] Meijer *et al.* reported the utility of a delicate balance between hydrophobic and hydrogen bond interactions in driving the supramolecular polymerization of monomers in water.[44,45] Hydrogen bonding and hydrophobic interactions acting in tandem stabilized water and organo-soluble supramolecular polymers.[46] Taking into consideration the above facts, in this piece of work we investigated the impact of substituted hydrophobic and hydrogen bonding moieties on viologen derivatives

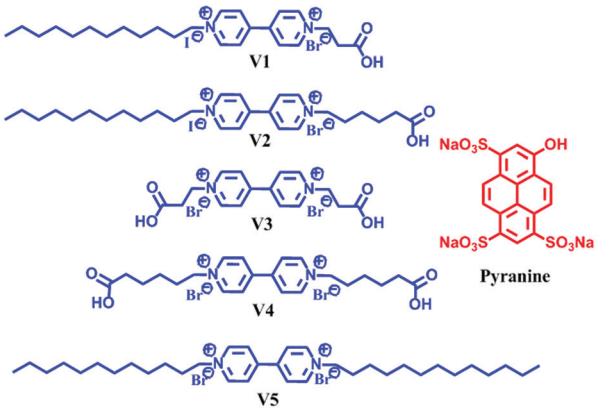

Scheme 1 Molecular structures of viologen derivatives **V1**, **V2**, **V3**, **V4**, **V5** and pyranine.

towards the CT interaction of viologen with pyranine. To pursue the study, we systematically designed and synthesized viologen derivatives, **V1**, **V2**, **V3**, **V4** and **V5** (Scheme 1). Molecules were designed in such a way that **V1** and **V2** were comprised of dodecyl chains on one nitrogen and alkyl carboxylic acid of variable length on the other nitrogen of 4,4′-bipyridine. **V3** and **V4** were endowed with alkyl carboxylic acids of varying length on nitrogen atoms of 4,4′-bipyridine in a symmetric fashion. **V5** was comprised of 4,4′-bipyridine quaternized on nitrogen atoms with dodecyl chains. Interactions between the viologens and pyranine were probed by electronic absorption and emission spectroscopy, NMR, dynamic light scattering (DLS), electrochemical, FTIR and electron microscopy techniques. Finally, the response of the formed CT aggregates was evaluated towards the recognition of adenosine nucleotides.

Experimental section

Materials

3-Bromopropanoic acid (99%), 6-bromopropanoic acid (99%), 1-iodododecane (99%), 1-bromododecane (98%), 6-hydroxy-1,3,8-pyrenetrisulfonic acid trisodium salt (99%) and 4,4′-bipyridine (99%) were obtained from Alfa Aesar. Acrylic acid (98%), hydrobromic acid (35%), potassium carbonate (99%), sodium hydroxide (99%) and potassium chloride (99%) were obtained from Avra Synthesis and used as received. Spectroscopic grade potassium bromide was obtained from Merck. Adenosine triphosphate disodium salt (98%), adenosine diphosphate disodium salt (98%) and adenosine monophosphate disodium salt (99%) were used as received from Sisco Research Laboratories. HPLC grade organic solvents were used as received. Ultrapure water having a resistivity of 18 MΩ cm (25 °C) was used for all purpose.

Instrumentation

NMR spectra were recorded on Bruker avance 400 and 500 MHz FT-NMR spectrometers. Chemical shift (δ) values were reported in parts per million (ppm) relative to the internal standard

tetramethylsilane (δ 0.00), D_2O (δ 4.79 ppm), $CDCl_3$ (δ 7.26 ppm) and DMSO-d_6 (δ 2.50 ppm). ^{13}C NMR chemical shift (δ) values were reported relative to the internal standard tetramethylsilane (δ 0.00), $CDCl_3$ (δ 77.0 ppm) and DMSO-d_6 (39.52 ppm). Coupling constants were reported in Hertz. ESI mass data were recorded on a 6545 Q-TOF LC/MS instrument from Agilent Technologies. UV-Visible absorbance spectra of solutions were recorded on a Shimadzu UV-3100 UV-Vis-NIR spectrophotometer at 21 °C. Fluorescence spectra were recorded using a JASCO FP-6300 spectrofluorometer. Helma cuvettes (path length = 1 cm) received from Sigma Aldrich were used to record absorption and fluorescence spectra. Electrochemical analyses were carried out in a CHI-910B electrochemical workstation (CH Instruments, USA). Measurements were performed in a three electrode cell comprising of glassy carbon, Ag/AgCl and platinum wire as working, reference and counter electrodes respectively. Solutions were purged with nitrogen gas before each experiment. FT-IR spectra were recorded on a JASCO FT/IR 4100 spectrometer. Field emission SEM images were recorded using a Hitachi S-4800 instrument. Particle size analysis of the CT aggregates was carried out using a Nano-ZS90 Zetasizer Nanoseries instrument procured from Malvern. Powder XRD patterns were recorded on a Bruker D8 Advance X-ray diffractometer using CuKα radiation (λ = 1.54178 Å). Thermogravimetric analysis (TGA) of the dried samples was conducted under a nitrogen atmosphere at a heating rate of 10 °C min^{-1} using a TGA Q500 V20.10 Build 36 instrument. Elemental analysis of the CT complexes was carried out using a PerkinElmer 2400 Series CHN analyser.

Synthesis

The details of the synthesis of viologen derivatives **V1**, **V2**, **V3**, **V4** and **V5** are provided in Scheme 2.

Synthesis of 1-dodecyl-4-(4-pyridyl)pyridinium iodide (1). To a refluxing solution of 4,4′-bipyridine (2 g, 12.8 mmol) in 30 mL of dry acetonitrile, 1-iododecane (2.73 mL, 12.8 mmol) was added dropwise over a time of 4 hours under an inert atmosphere. The mixture was allowed to reflux for 24 hours. After cooling to room temperature, the solution was filtered and the filtrate was evaporated to obtain the crude solid which was triturated with hot hexane to obtain 1 as a red solid (2.2 g, 58% yield). ^1H NMR (400 MHz, $CDCl_3$, 25 °C): δ = 9.47–9.46 (d, J = 6.4 Hz, 2H), 8.87–8.85 (d, J = 5.6 Hz, 2H), 8.40–8.38 (d, J = 6.4 Hz, 2H), 7.72–7.71 (d, J = 5.6 Hz, 2H), 4.97–4.93 (t, J = 7.6 Hz, 2H), 2.08–2.04 (t, J = 7.2 Hz, 2H), 1.34–1.22 (m, 18H), 0.87–0.84 (t, J = 6.8 Hz, 3H). ^{13}C NMR (100 MHz, $CDCl_3$, 25 °C): 153.9, 151.6, 145.6, 140.9, 126.1, 121.6, 62.1, 32.0, 31.9, 29.7, 29.6, 29.5, 29.4, 29.1, 26.2, 22.8, 14.2 (see Fig. S1 and S2, ESI†).

Synthesis of 1-(2-carboxyethyl)-1′-dodecyl-4,4′-bipyridinium bromide iodide (V1). A mixture of compound **1** (0.5 g) and 3-bromopropanoic acid (0.75 g) was dissolved in dry acetonitrile under an inert atmosphere and refluxed for 72 hours. The precipitate was collected by filtration and washed with hot acetonitrile and dried under vacuum to obtain pure **V1** as an orange red solid (0.5 g, 74% yield). ^1H NMR (400 MHz, DMSO-d_6, 25 °C): δ = 9.41–9.40 (d, J = 6.4 Hz, 4H), 8.80–8.78 (d, J = 6.4 Hz, 4H), 4.91–4.88 (t, J = 6.6 Hz, 2H), 4.71–4.67 (t, J = 7.4 Hz, 2H), 3.18–3.15 (t, J = 6.4 Hz, 2H), 1.97 (m, 2H), 1.30–1.23 (m, 18H), 0.86–0.82 (t, J = 6.6 Hz, 3H). ^{13}C NMR (100 MHz, DMSO-d_6, 25 °C): δ = 171.6, 148.9, 148.6, 146.4, 145.8, 126.7, 126.3, 60.9, 56.7, 34.4, 31.3, 30.8, 29.0, 29.0, 28.9, 28.8, 28.5, 25.5, 22.1, 14.0 (*cf.* Fig. S3 and S4, ESI†). ESI-HRMS: calculated for $C_{25}H_{38}IBrN_2O_2$: 606.1144; found m/z 607.1196 $(M + H)^+$, 624.1660 $(M + NH_4)^+$.

Synthesis of 1-(5-carboxypentyl)-1′-dodecyl-4,4′-bipyridinium bromide iodide (V2). A mixture of compound **1** (0.5 g) and 6-bromohexanoic acid (0.5 g) was dissolved in dry acetonitrile under an inert atmosphere and refluxed for 72 hours. The precipitate was collected by filtration and washed with hot acetonitrile and dried under vacuum to obtain **V2** as an orange red solid (0.52 g, 72.6% yield). ^1H NMR (400 MHz, DMSO-d_6, 25 °C): δ = 12.03 (s, broad), 9.43–9.41 (d, J = 6.8 Hz, 4H), 8.82–8.80 (d, J = 6 Hz, 4H), 4.72–4.70 (t, J = 6 Hz, 4H), 2.23–2.22 (t, J = 7.2 Hz, 2H), 2.02–1.98 (t, J = 7.2 Hz, 4H), 1.58–1.53 (m, J = 7.2 Hz, 2H), 1.32–1.24 (m, 20 H), 0.86–0.83 (t, J = 6.6 Hz, 3H). ^{13}C NMR (100 MHz, DMSO-d_6, 25 °C): δ = 174.3, 148.5, 145.8, 126.6, 60.8, 60.6, 33.3, 31.3, 30.7, 30.4, 29.0, 28.9, 28.8, 28.7, 28.4, 25.4, 24.9, 23.8, 22.1, 14.2 (see Fig. S5 and S6, ESI†). ESI-HRMS: calculated for $C_{28}H_{44}IBrN_2O_2$: 646.1631; found, 669.1518 $(M + Na)^+$.

Synthesis of 1,1′-bis(2-carboxyethyl)4,4′-bipyridin-1,1′-diium bromide (V3). A mixture of 3-bromopropanoic acid (1.8 g) and 4,4′-bipyridine (0.2 g) was dissolved in 60 mL of dry acetonitrile under an inert atmosphere and refluxed over a period of 72 hours. The reaction mixture was cooled to room temperature and the solution was filtered. The crude solid obtained was triturated with hot acetonitrile, filtered and dried under vacuum to obtain pure **V3** as a pale white solid (0.2 g, 33.89% yield). ^1H NMR (400 MHz, DMSO-d_6, 25 °C): δ = 12.8 (s, broad), 9.43–9.41 (d, J = 6.4 Hz, 4H), 8.81–8.80 (d, J = 6.8 Hz, 4H), 4.91–4.88 (t, J = 6.6 Hz, 4H), 3.19–3.16 (t, J = 6.6 Hz, 4H)

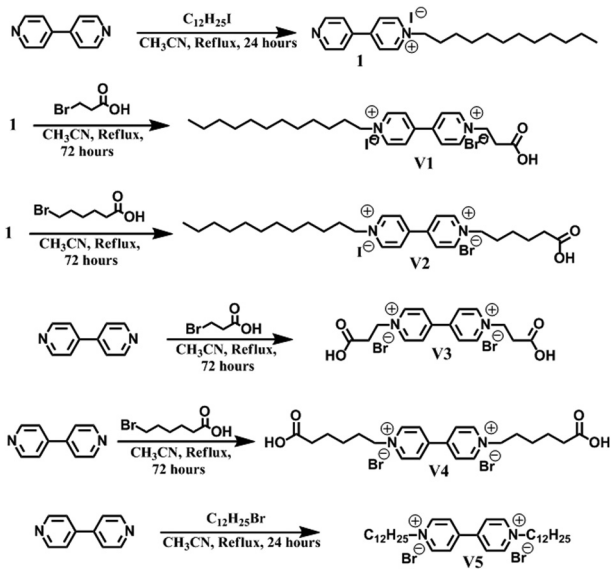

Scheme 2 Synthetic scheme of viologen derivatives **V1**–**V5**.

^{13}C NMR (125 MHz, DMSO-d_6, 25 °C): δ = 171.5, 148.8, 146.4, 126.3, 56.6, 34.3 (see Fig. S7 and S8, ESI†). ESI-HRMS: calculated for $C_{16}H_{18}Br_2N_2O_4$: 459.9649; found, 460.9690 $(M + H)^+$.

Synthesis of 1,1′-bis(5-carboxypentyl)4,4′-bipyridin-1,1′-diium bromide (V4). A mixture of 6-bromohexanoic acid (1.2 g) and 4,4′-bipyridine (0.25 g) was dissolved in 20 mL of dry acetonitrile under an inert atmosphere and refluxed over a period of 72 hours. The reaction mixture was cooled to room temperature and the solution was filtered. The crude solid obtained was washed with hot acetonitrile and dried under vacuum to obtain pure **V4** as a pale white solid (0.65 g, 74.3% yield). ^{1}H NMR (400 MHz, DMSO-d_6, 25 °C): δ = 12.04 (s, broad), 9.49–9.47 (d, J = 8 Hz, 4H), 8.88–8.86 (d, J = 8 Hz, 4H), 4.77–4.73 (t, J = 8 Hz, 4H), 2.29–2.25 (t, J = 8 Hz, 4H), 2.07–1.99 (q, J = 8 Hz, 4H), 1.64–1.56 (q, J = 8 Hz, 4H), 1.41–1.37 (t, J = 8 Hz, 4H). ^{13}C NMR (100 MHz, DMSO-d_6, 25 °C): δ = 174.3, 148.5, 145.8, 126.6, 60.6, 33.3, 30.4, 24.9, 23.8 (see Fig. S9 and S10, ESI†). ESI-HRMS: calculated for $C_{22}H_{30}Br_2N_2O_4$: 544.0623; found, m/z 546.0643 $(M + H)^+$, 567.0524 $(M + Na)^+$.

Synthesis of 1,1′-didodecyl-4,4′-bipyridin-1,1′-diium bromide (V5). 4,4′-Bipyridine (0.39 g) and 1-bromododecane (1.5 g) were dissolved in 25 mL of dry acetonitrile and refluxed over a period of 48 hours. The pale yellow solid obtained was filtered and washed with hot CH_3CN (1.0 g, 61%). ^{1}H NMR (400 MHz, DMSO-d_6, 25 °C): δ = 9.41–9.39 (d, J = 8 Hz, 4H), 8.81–8.79 (d, J = 8 Hz, 4H), 4.71–4.67 (t, J = 8 Hz, 4H), 1.98 (q, 4H), 1.31–1.24 (m, 36 H), 0.86–0.83 (t, 6 Hz, 3H). ^{13}C NMR (400 MHz, DMSO-d_6, 25 °C): 148.5, 145.7, 126.6, 60.9, 31.3, 30.7, 29.0, 28.9, 28.8, 28.7, 28.4, 25.4, 22.1, 14.0 (see Fig. S11 and S12, ESI†). ESI-HRMS: calculated for $C_{34}H_{58}Br_2N_2$: 652.2969; found, m/z 675.2860 $(M + Na)^+$.

Results and discussion

^{1}H NMR and ^{13}C NMR spectra of the synthesised compounds in Scheme 2 clearly evinced the formation of bipyridine derivatives where aromatic ring protons of bipyridine resonated within a chemical shift range of 9.5–8.4 ppm. While compounds **V1** to **V4** exhibited good solubility in water, **V5** was insoluble in water. The bisbromide analogues of **V1** and **V2**, namely **V6** and **V7**, synthesized initially, exhibited partial solubility in water. Synthesis and characterization details of **V6** and **V7** are given in Fig. S13–S17, ESI.† Hence **V1** and **V2** with bromide and iodide as counter anions, exhibiting good solubility in water, were used for the investigation.

Characteristic aggregation in the viologen–pyranine charge transfer complexes

The interaction of pyranine with clear and transparent aqueous solutions of **V1** and **V2** gave rise to a stable suspension, whereas its interaction with **V3** and **V4** resulted in a clear solution without any aggregation, exhibiting a change in colour (Fig. 1). The aggregates obtained for [**V1**–Pyr] and [**V2**–Pyr] were robust enough to be isolated by filtration. To the best of our knowledge, such a phenomenon of isolating CT aggregates by filtration is yet to be reported. Simultaneously, emission from pyranine solution was quenched upon addition of viologen derivatives, as revealed in Fig. 2. Visuals of similar behaviour from **V2** and **V4** with pyranine are presented in Fig. S18, ESI.†

Do counter ions play a role in aggregation?

In order to answer this, CT aggregates were prepared and studied for their properties. 10 mL of 10^{-2} M aqueous solutions of viologen derivatives (**V1**, **V2**, **V6** and **V7**) and 10 mL of 10^{-2} M aqueous solution of pyranine were mixed thoroughly under stirring. CT complexes formed were filtered through a Whatman 40 filter paper, and washed with copious amounts of water till the filtrate answered negative towards halides (tested with aqueous silver nitrate for precipitation) and pyranine (tested for emission under UV light). CT aggregates thus obtained were dried under vacuum and used for further analysis (Fig. S19, ESI†).

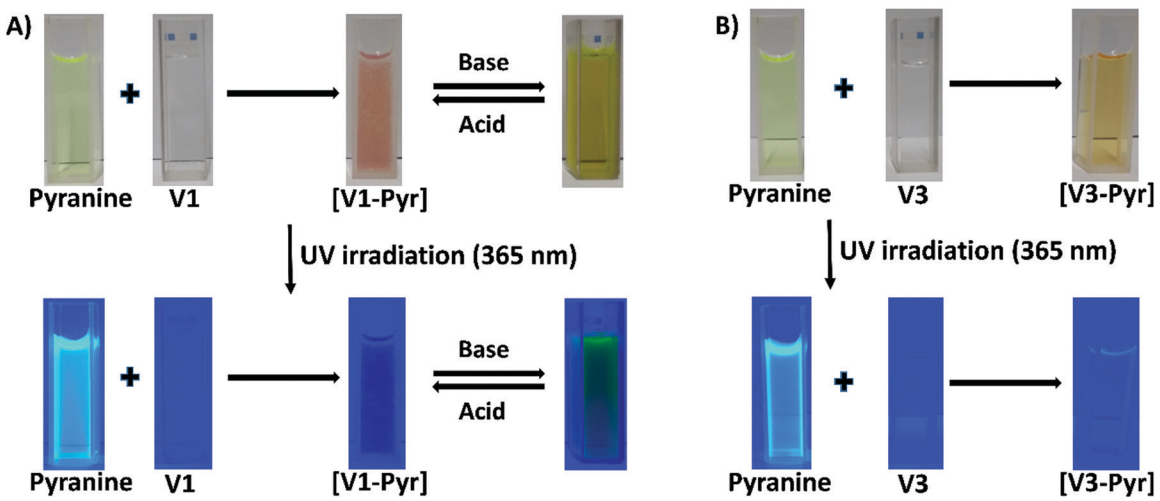

Fig. 1 Visual appearance of the CT aggregates of (A) **V1**–pyranine and (B) **V3**–pyranine, and their response to variation in pH. Images of **V2**–pyranine and **V4**–pyranine CT aggregates are incorporated in ESI,† Fig. S14.

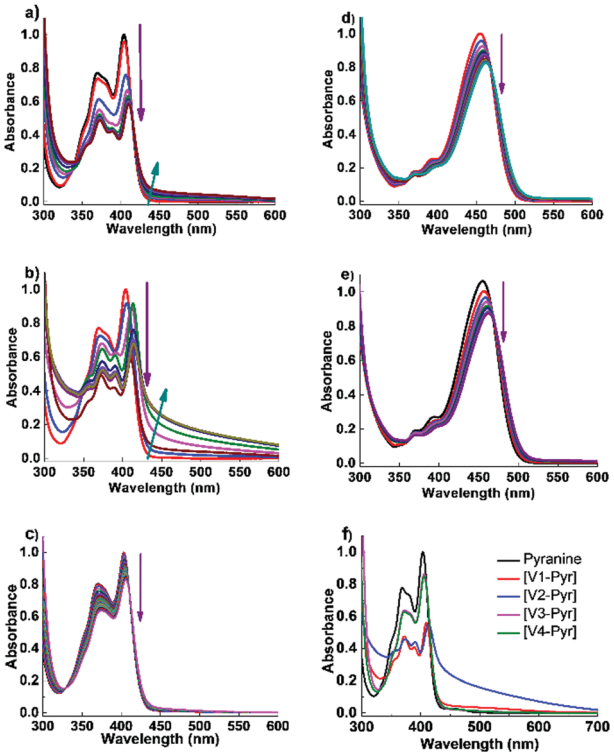

Fig. 2 UV-Visible absorption spectra of 50 μM pyranine upon successive addition of (a) **V1** (0 to 3 eq.), (b) **V2** (0 to 2 eq.) (c) **V4** (0 to 5 eq.), (d) **V1** (0 to 6 eq.) at pH = 12, (e) **V2** (0 to 6 eq.) at pH = 12 and (f) comparison of the absorption spectra of [**V1**–Pyr], [**V2**–Pyr], [**V3**–Pyr] and [**V4**–Pyr] in water. The direction of the arrows indicates the change in the absorbance of pyranine upon increasing addition of viologens.

In order to evaluate the impact of self-assembly on the properties of the resultant CT complexes, PXRD, TG–DTA and CHN analyses were carried out. PXRD patterns exhibited by the CT aggregates were quite distinct from those of their precursors (Fig. S20a, ESI†). Viologen derivatives **V1** and **V2** and pyranine exhibited sharp crystalline peaks whereas the [**V1**–Pyr] CT aggregates showed a broad peak indicating the amorphous nature of the complex, in stark contrast with the crystalline nature of the precursors. The [**V2**–Pyr] CT complex on the other hand gave rise to mixed sharp and broad features, indicating the co-existence of crystalline and amorphous domains in CT aggregates. Further, TG–DTA analysis of the precursors and CT complexes revealed interesting features (Fig. S21, ESI†). Variation in the thermal behaviour between the precursors and CT aggregates resulted not only due to the formation of cofacially stacked CT complexes but also because of the elimination of sodium, bromide and iodide ions as water soluble by-products, leaving behind a new chemical entity whose property was different from that of its precursors. The experimentally observed CHN content of CT aggregates was compared with the theoretically calculated CHN content of 1 : 1 (anionic) and 3 : 2 (neutral) complexes of viologen and pyranine. The results for [**V1**–Pyr] and [**V2**–Pyr] ruled out the existence of counter ions such as bromide, iodide and sodium in the aggregates (Tables S1 and S2, ESI†).

In order to analyse the impact of counter anions on self-assembly, the analogues of **V1** and **V2** with bromide ion alone as the counter anion (**V6** and **V7**) were tested for CT complexation with pyranine. As mentioned previously, **V1** and **V2** comprising of bromide and iodide as counter anions exhibited better solubility than **V6** and **V7**. The interaction of **V6** (Br^-, Br^-) and **V7** (Br^-, Br^-) derivatives with pyranine in water formed water insoluble CT aggregates, similar to that of **V1** (I^-, Br^-) and **V2** (I^-, Br^-). PXRD and TG–DTA features of [**V6**–Pyr] and [**V7**–Pyr] CT aggregates were also similar to that of [**V1**–Pyr] and [**V2**–Pyr] CT aggregates without any marked differences (Fig. S21 and S22, ESI†). Further, in CHN analysis, [**V6**–Pyr] and [**V7**–Pyr] CT aggregates exhibited a higher level of carbon content which could be attributed to the insoluble **V6** and **V7** precursors trapped in the aggregates (Tables S3 and S4, ESI†). These observations clearly indicate that apart from solubility, counter anions did not wield considerable influence over CT complexation and the properties of CT aggregates.

UV-vis and fluorescence spectroscopy of the CT aggregates

In order to acquire an insight into CT interactions between the viologen derivatives and pyranine, electronic absorption and emission spectra (Fig. 2 and 3) in ultrapure water were recorded. Solutions of viologen derivatives were colorless and exhibited absorption bands within the range 250 to 270 nm. No change in their optical properties upon varying pH was noted (Fig. S23a, ESI†). The absorption maxima of pyranine observed in water at 370 nm and 404 nm diminished considerably at basic pH along with the appearance of a new absorption band at 456 nm, characteristic of the deprotonated form of pyranine (Fig. S23b, ESI†). Addition of **V1** or **V2** to a 50 μM solution of pyranine resulted in visually discernible aggregation. In Fig. 2a, the absorption maximum of pyranine at 370 nm and 404 nm gradually decreased in intensity due to the formation of CT aggregates. A pattern similar to that of **V1** was also observed for **V2** (Fig. 2b), indicating charge transfer complexation between the derivatives of viologen and pyranine. In the case of [**V1**–Pyr] and [**V2**–Pyr], the red shift of pyranine absorption peaks was accompanied by a concomitant decrease in the intensity of pyranine absorption. Furthermore, for **V1** or **V2**, the observed levelling-off of the absorption tails at longer wavelength was attributed to Mie scattering,[47,48] which was even more pronounced for the [**V2**–Pyr] CT complex in water. Mie scattering results when the size of the scattering aggregates is of the same order of magnitude as the wavelength of the incident light.[49] When the titration was carried out at basic pH (pH = 12), due to deprotonation of the carboxylic acid group of viologens, no aggregates were formed in the case of **V1** or **V2**, resulting in homogeneous solutions (Fig. 2d and e).

In order to assess the role of substituents, we evaluated the response of **V3** and **V4** towards pyranine. **V3** and **V4** were comprised of symmetrically substituted carboxypropyl and carboxypentyl groups on 4,4′-bipyridinium moieties without hydrophobic dodecyl chains. Addition of **V3** or **V4** to the pyranine solution resulted in a meagre bathochromic shift of the pyranine absorption from 404 nm to 407 nm (Fig. 2e and Fig. S24a, ESI†).

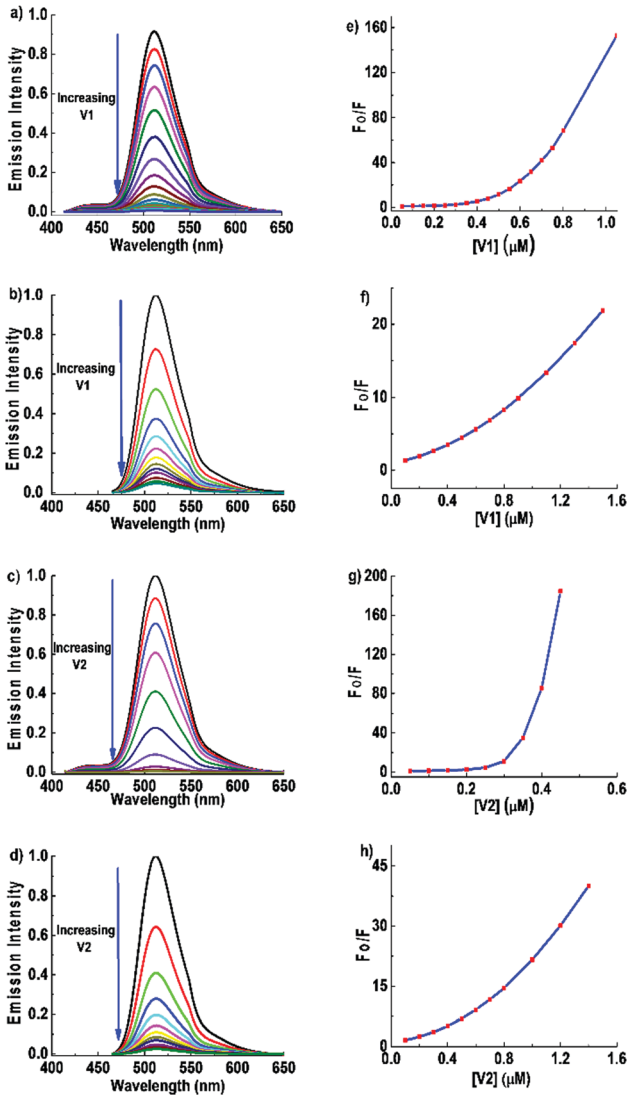

Fig. 3 Emission spectra of pyranine in the presence of (a) **V1**, (b) **V1** at pH = 12, (c) **V2**, (d) **V2** at pH = 12; (e–h) Stern–Volmer plots for the corresponding fluorescence spectra. Excitation wavelength: 404 nm in water; 456 nm at basic pH.

The interaction of **V3** or **V4** with pyranine did not generate any aggregates like that of [**V1**–Pyr] and [**V2**–Pyr], emphasizing the role of hydrophobic dodecyl chains which played a pivotal role in driving the aggregation in the case of **V1** and **V2**. Scattering was absent for [**V3**–Pyr] and [**V4**–Pyr], unlike that of [**V1**–Pyr] and [**V2**–Pyr]. Fig. 2f gives a comparative account of CT complexation between the derivatives of viologen and pyranine; expanded spectra are given in Fig. S24b, ESI.†

Pyranine has its absorption maximum centred at 404 nm in ultrapure water and at 456 nm at pH = 12. Upon excitation at either of the wavelengths, the emission maximum appeared at 512 nm. Stepwise addition of **V1** or **V2** to 50 μM pyranine solution quenched the emission intensity of pyranine due to the formation of the CT aggregates (Fig. 3). Stern–Volmer plots in Fig. 3(e–h) reveal the impact of pH on CT interactions. Two distinct regions are noted with the emission intensity ratio remaining constant at lower quencher concentrations followed by its steep rise at higher concentrations (Fig. 3e and g). At basic pH, the Stern–Volmer plots (Fig. 3f and h) showed a steep exponential rise in the curve upon successive addition of viologens to pyranine. Three equivalents of **V1** were required to quench the emission of pyranine up to 10% of its original intensity in water, whereas, at basic pH, six equivalents of **V1** were required to bring about the decrease. Two and four equivalents of **V2** were required to quench the emission of pyranine to one-tenth of its original intensity in ultrapure water and basic pH respectively. At basic pH, deprotonation of pyranine rendered it tetra-anionic which demanded a larger amount of viologen to bring about the emission quenching.

Probing CT-induced aggregation *via* NMR titrations

NMR is a versatile tool in supramolecular chemistry to probe non-covalent interactions such as host–guest interactions, CT complexation and various other modes of molecular recognition. Here, the CT complexation between viologen derivatives and pyranine was investigated *via* ^{1}H NMR spectroscopy. Aromatic protons in viologen derivatives of **V1** and **V2** (Fig. 4a and 5A(a)) resonated at 9.1 ppm and 8.5 ppm in D_2O and the chemical shift of the protons was unaffected by the addition of K_2CO_3. Protons in pyranine resonated from 9.2 ppm to 8.3 ppm in D_2O (Fig. 4b), and from 8.8 to 7.9 upon addition of K_2CO_3 (Fig. 5B(b)) due to deprotonation of pyranine. Addition of pyranine to **V1** in D_2O resulted in disappearance of resonances of the protons of **V1** and pyranine due to aggregation. In the presence of K_2CO_3, the above suspension resulted in a clear solution accompanied by regeneration of NMR signals observed at upfield chemical shifts with significant broadening (Fig. 4d), relative to that of individual donor and acceptor. Therefore, to further deepen the understanding of CT-induced aggregation, we carried out NMR titrations at basic pH, achieved by addition of K_2CO_3 to D_2O, prior to addition of CT components.

In Fig. 5A, a gradual decrease in the intensity of resonances of the protons of **V2** was noticed when pyranine was added

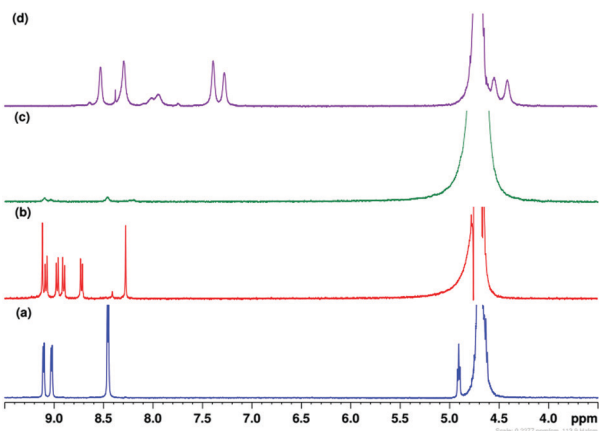

Fig. 4 ^{1}H NMR spectra in D_2O of (a) **V1**, (b) pyranine, (c) [**V1**–pyranine], (d) [**V1**–pyranine] + K_2CO_3.

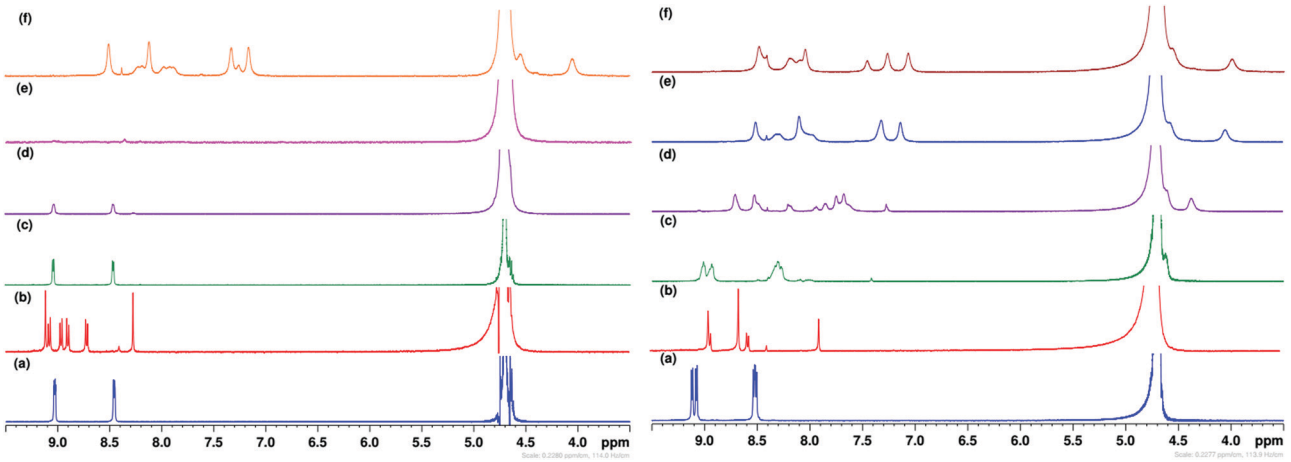

Fig. 5 (A) ^{1}H NMR spectra in D_2O of (a) **V2**, (b) pyranine, (c–e) **V2** + 0.25, 0.50, and 0.75 equivalents of pyranine, (f) **V2** + 0.75 equivalent of pyranine + K_2CO_3. (B) ^{1}H NMR spectra in K_2CO_3 + D_2O of (a) **V2**, (b) pyranine, (c–f) **V2** + successive addition of 0.25, 0.50, 0.75 and 1.0 equivalents of pyranine.

successively to a solution of **V2** in D_2O. With 0.75 eq. pyranine, the resonances of the protons corresponding to **V2** disappeared due to the formation of CT aggregates (Fig. 5A(e)). Resonances of the pyranine protons also did not appear in NMR spectra due to aggregation. However, addition of base to the [**V2**–Pyr] suspension resulted in the disruption of H-bonds leading to protons of CT complexes resonating at upfield values (Fig. 5A(f)) relative to their precursors, as also seen in the case of [**V1**–Pyr]. This upfield shift of protons is a clear indication of cofacial π-stacking[39] in [**V2**–Pyr] and [**V1**–Pyr], arising as a result of higher electron density build-up (and hence a greater shielding) due to the aromatic π electrons, situated above or below the respective protons. Pyranine was added in small portions up to 1.0 equivalent to **V2** in basic solution. With increasing concentration of pyranine, proton resonances corresponding to both the components underwent a similar upfield shift accompanied by peak broadening, indicative of the characteristic face-to-face stacking arrangement in the aggregate (Fig. 5b). The methylene group directly attached to the nitrogen atom of bipyridine in **V2** and resonating at 4.95 ppm was shifted upfield to 4.3 ppm, which provided further indication of CT complexation between viologen and pyranine. In the case of **V3** or **V4**, which lacked dodecyl groups, addition of pyranine in D_2O only led to a upfield shift of protons in both viologen and pyranine (Fig. S25, ESI†), implying the prevalence of CT interactions. Here, the absence of turbidity ruled out the formation of any defined aggregate for **V3** or **V4**, as shown in Fig. 1B and Fig. S18, ESI.†

Particle size analysis of the aggregates

Dynamic light scattering (DLS) has been employed to determine the hydrodynamic size of macromolecules, proteins, and micro- and nanoparticles. In the present work, DLS measurements were made upon stepwise addition of viologen derivatives **V1** or **V2** to a 50 μM solution of pyranine. The size of the aggregates increased upon gradual addition of viologens as shown in Fig. 6. Successive addition of **V1** to pyranine in water up to 1 equivalent led to the formation of 750 nm aggregates

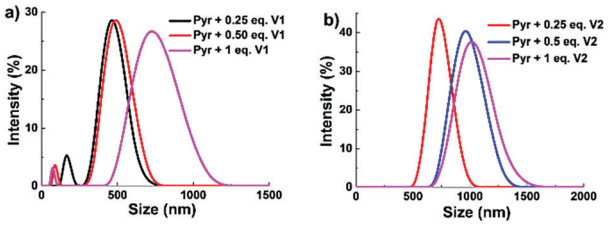

Fig. 6 Particle size analysis of (a) **V1**–Pyr and (b) **V2**–Pyr CT aggregates in aqueous solution.

(Fig. 6a). In the case of **V2**, the successive addition of pyranine resulted in an aggregate size of 750 nm, reaching a maximum of 1120 nm for 1 eq. pyranine (Fig. 6b). Further addition of viologens did not have any impact on the size of the aggregates.

Redox behaviour of viologen–pyranine supramolecular aggregates

Viologens are excellent redox mediators exhibiting diverse redox states (dication, radical cation and neutral) upon pulsing appropriate redox[19] or chemical[20] stimuli. The cyclic voltammetry of viologen derivatives in aqueous solution exhibited two redox couples as a result of two consecutive one electron reduction processes (Fig. S26, ESI†). As discussed in the previous sections, viologen derivatives **V1** to **V4** upon interaction with pyranine exhibited complexation with distinct properties, characteristic of the substituents on viologen. To investigate the redox behaviour of CT complexation, cyclic voltammetry was carried out in aqueous solution using 0.1 M KCl as the supporting electrolyte. **V1** exhibited two reduction peaks at −0.50 V and −0.74 V and the corresponding oxidation peaks at −0.69 V and −0.40 V respectively (*vide* Fig. 7a). Stepwise addition of pyranine to **V1** led to aggregation, reflected by a significant drop in the peak current due to decreased availability of free **V1** in solution. Trends similar to **V1** were observed for **V2** (Fig. 7b) with respect to peak current upon successive addition of the donor. Further, base addition to the

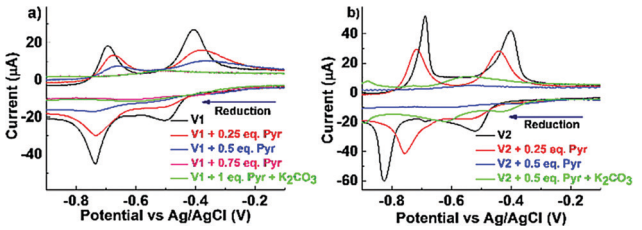

Fig. 7 Cyclic voltammograms of (a) **V1** and (b) **V2** upon interaction with pyranine in aqueous media with 0.1 M KCl supporting electrolyte. WE: glassy carbon electrode, aux. electrode: Pt, RE: Ag/AgCl.

CT suspensions of [**V1**–Pyr] and [**V2**–Pyr] resulted in their dissolution, accompanied by the absence of any considerable redox current. This could be attributed to the decreased diffusion coefficients of the complexed viologen derivatives. A good compliance was noticed for the first reduction peaks of **V1** and **V2** at −0.50 V and −0.52 V respectively. Nevertheless, a more negative potential for the second reduction peak of **V2** at −0.82 V *vs.* −0.74 V for **V1** implied the influence of the length of the alkyl chain attached to the carboxylic acid moiety of the viologen; a larger chain length brought in difficulty in reduction.

FT-IR spectroscopy of the CT aggregates

FT-IR spectra of viologen derivatives, pyranine and CT aggregates were recorded to investigate the impact of supramolecular interactions, especially the H-bonding (Fig. S27 and S28, ESI†). The viologen derivatives (**V1** and **V2**) exhibited broad absorption bands from 3300 cm^{-1} to 2400 cm^{-1}, characteristic of ν_s(O–H) stretching vibration of the carboxylic acid moiety, overlapped with the aromatic and aliphatic C–H stretching bands. Further, their ν_s(C═O) bands appeared at 1736 cm^{-1} and 1732 cm^{-1} for **V1** and **V2**. A lower wavenumber frequency shift of the ν_s(C═O) band for the [**V1**–Pyr] and [**V2**–Pyr] aggregates to 1723 cm^{-1} implied the prevalence of intermolecular H-bonds in driving aggregation in synergy with hydrophobic interactions towards the CT aggregates.

Scanning electron microscopy of the supramolecular aggregates

The visually discernible charge transfer complexed aggregates of [**V1**–Pyr] and [**V2**–Pyr] were examined for their geometry using SEM (*vide* Fig. 8 and 9). Images were acquired for the drop cast films of the corresponding suspensions on clean ITO substrates. Pristine **V1** and **V2** exhibited distorted and stacked flake like structures (Fig. S29, ESI†) whereas [**V1**–Pyr] aggregates gave rise to cuboidal particles (Fig. 8). At lower concentrations, aggregates appeared to be oblique without a predefined shape. SEM images of [**V2**–Pyr] aggregates revealed an interconnected network of fibres (Fig. 9). Upon dilution, the morphology of the aggregates was retained with discrete particles scattered over the fibrous matrix. These self-assembled aggregates substantiated the Mie scattering observed in the absorption spectra of [**V1**–Pyr] and [**V2**–Pyr] complexes (Fig. 2). Addition of base to the suspension of [**V1**–Pyr] and [**V2**–Pyr] aggregates led to dissolution with the concomitant disappearance of Mie scattering in

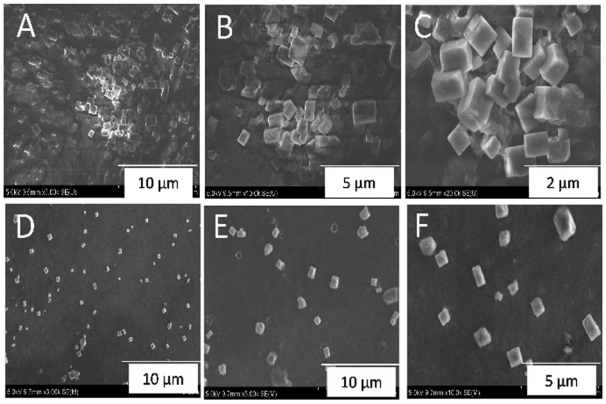

Fig. 8 SEM images of **V1**–Pyr CT aggregates: (A–C) higher concentration (5×10^{-3} M), (D–F) lower concentration (5×10^{-4} M).

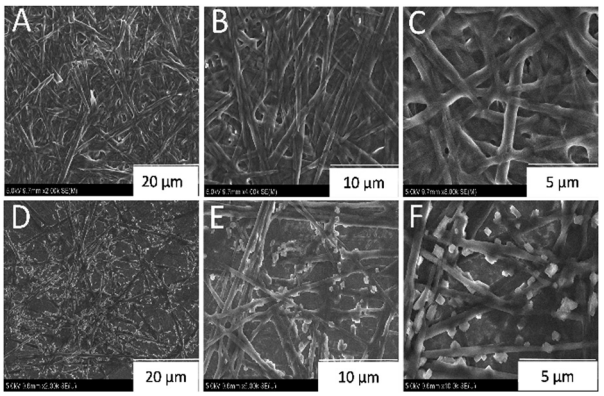

Fig. 9 SEM images of **V2**–Pyr CT aggregates: (A–C) higher concentration (5×10^{-3} M), (D–F) lower concentration (5×10^{-4} M).

absorption spectra. However, [**V3**–Pyr] and [**V4**–Pyr] complexes remained soluble in water irrespective of pH. The solution of the [**V4**–Pyr] complex drop cast on a ITO plate gave rise to structures without any characteristic morphology (Fig. S29(E), ESI†).

It is remarkable to observe water insoluble cuboidal and fibrous micro- and nanostructures synthesized from water soluble precursors. Such structures are often fabricated by adopting a top-down lithographic approach[50] or by modifying the environment of the corresponding precursors by suitable stimuli such as pH, surfactants, metal ions, *etc.*[51,52] Deprotonation driven solubilization of [**V1**–Pyr] and [**V2**–Pyr] aggregates under physiological conditions (pH greater than 7) in the present study further provides an opportunity to utilize such aggregates as templates towards fabricating nanomaterials.[53]

CT complexes often give rise to nanostructures such as fibers, micelles, tubes, spheres, rods, sheets, *etc.*[54] To the best of our knowledge, we are yet to come across CT interactions between a donor and an acceptor giving rise to cuboidal aggregates in aqueous medium. Recent reports demonstrated that cuboidal nanoparticles exhibit better internalization in HeLa cells and breast cancer cell lines than their spherical counterparts.[55,56] The nanosized cuboidal and tubular aggregates

from [**V1**–Pyr] and [**V2**–Pyr] in the present investigation exhibited good solubility at physiological pH which makes them potential candidates in the investigation of their utility in biological systems.

Mechanism of aggregation

In view of the results obtained from the above experiments, the mechanism of aggregation in [**V1**–Pyr] and [**V2**–Pyr] CT complexes and absence of aggregation in [**V3**–Pyr] and [**V4**–Pyr] in water are explained as follows:

(i) Water soluble viologen derivatives **V1** to **V4** possess a complementary electrostatic nature with respect to pyranine which formed CT complexes upon interaction, exemplified by quenching of pyranine emission upon addition of the viologen derivative. CT complexation between **V1** to **V4** and pyranine resulted in an alternate, cofacially stacked architecture (Scheme 3). This face-centred stacking maximized the decrease in the aromatic surface area of the complex exposed to water molecules, resulting in desolvation.[57,58] As a result of electrostatic complementarity between viologen and pyranine, hydrophobic flat surfaces of aromatic molecules stacked alternately with elimination of counter anions as corresponding sodium halides in water.

(ii) Donor–acceptor interaction driven alternate stacking resulted in increased local concentration of dodecyl chains. By virtue of their hydrophobic nature, the association among alkyl chains steered further exclusion of water molecules in their vicinity alongside of the donor–acceptor stacking driven desolvation of aromatic faces.

(iii) Alkyl carboxylic acids of varying length in **V1** and **V2** induced the aggregation of [**V1**–Pyr] and [**V2**–Pyr] CT complexes by intermolecular hydrogen bonds between terminal carboxylic acid moieties of viologen derivatives. The H-bonding interaction in concurrence with hydrophobic and CT interactions amplified the extent of supramolecular polymerization, generating a stable suspension. Emergence of Mie scattering in UV spectra clearly evinced the formation of aggregates in water. UV spectra of [**V2**–Pyr] CT complexes in water exhibited greater Mie scattering in comparison to that of [**V1**–Pyr] due to enhanced hydrophobicity of **V2** resulting in larger particles.

(iv) Viologens **V3** and **V4** comprising of alkyl carboxylic acids tethered to bipyridine are devoid of dodecyl chains. Their interaction with pyranine resulted in CT complexation. Yet, the CT interaction failed to give rise to aggregates. The presence of hydrogen bonding carboxylic acid groups in **V3** or **V4**, in addition to charge-transfer and electrostatic binding, was not sufficient to bolster aggregation similar to that of [**V1**–Pyr] and [**V2**–Pyr]. Absence of hydrophobic dodecyl chains hindered the formation of aggregates.

(v) The viologen derivative **V5** comprising exclusively of hydrophobic dodecyl chains was insoluble in water. However, the literature reports that the interaction between water soluble viologen derivatives with shorter alkyl chains and pyranine resulted in 1-D nanofibers[39] and hydrogels.[40] Such interactions never resulted in visually discernible particle formation similar to that of [**V1**–Pyr] and [**V2**–Pyr]. The absence of hydrogen bonding carboxylic acid moieties in **V5** clearly hindered the formation of aggregates.

(vi) [**V1**–Pyr] aggregates were predominantly cuboidal in geometry, while [**V2**–Pyr] aggregates revealed the coexistence of cuboidal and fibrous aggregates. This difference in morphology could be attributed to variation in the length of the alkyl carboxylic acids appended onto the nitrogen atoms of 4,4′-bipyridine. A lengthier alkyl carboxylic acid in **V2** provided an additional window for alkyl chain entanglement in addition to H-bonding, which resulted in fibrous aggregates. At lower concentrations, [**V2**–Pyr] revealed coexistence of fibrous and geometrically less-defined aggregates. The structure – interaction quotients have been combined to arrive at the most probable mechanism of self-assembly, as schematically represented in Scheme 3.

(vii) Considering all the above features, we propose that the cooperativity among hydrophobic, hydrogen bonding and CT interactions between the donor and acceptor gave rise to supramolecular aggregates. Hydrophobic and H-bonding interactions reinforced each other concomitant with CT stacking, leading to supramolecular polymerization. Addition of base to CT aggregates of [**V1**–Pyr] and [**V2**–Pyr] in water led to disaggregation resulting in true solution. Further addition of acid to the above solution regenerated the aggregates signifying the importance of hydrogen bonding (Fig. 1 and Scheme 3). Lack of hydrophobic dodecyl chains in the case of **V3** and **V4** prohibited aggregation of [**V3**–Pyr] and [**V4**–Pyr], whereas lack of hydrogen bonding carboxylic acid in **V5** rendered it insoluble in water. This emphasizes the fact that neither the hydrogen bonding motif nor the hydrophobic dodecyl chain can induce aggregation independently. A synergy between multiple non-covalent interactions is vital in realizing such functional systems.

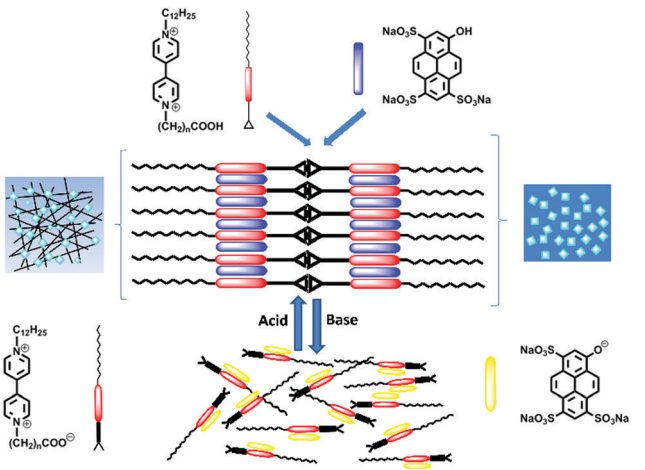

Scheme 3 Schematic representation of charge-transfer complexation induced self-assembly of amphiphilic viologen derivatives and pyranine and the response of the assembly towards pH.

Nucleotide recognition by charge-transfer aggregates

Recognition and sensing of biologically relevant anionic species like phosphates and nucleotides enjoy special privilege due

to their significance in biological functions of various organelles.[59] Any abnormality in their concentration in biological systems provides a direct indication of biological disorders. CT complexes of viologen–pyranine were reported as fluorescent sensors towards a variety of nucleotides.[34,35] Inspired by the above reports, we investigated the susceptibility of adenine nucleotides towards displacing pyranine from CT aggregates of [**V1**–Pyr] and [**V2**–Pyr] in water.

Suspensions of [**V1**–Pyr] and [**V2**–Pyr] in water were examined towards the change in their photophysical properties with respect to their interaction with ATP, ADP and AMP (Fig. 10a and b). Addition of ATP and ADP over a concentration range from 10^{-5} M to 10^{-2} M did not bring about any change in the emission behaviour of [**V1**–Pyr] and [**V2**–Pyr] suspensions. However, addition of AMP to [**V1**–Pyr] and [**V2**–Pyr] suspensions led to disaggregation of the aggregates resulting in a clear yellow solution accompanied by an increase in the emission intensity at 512 nm (Fig. 10c and Fig. S30, ESI†). Moreover, the [**V3**–Pyr] solution did not exhibit any response towards ATP, ADP and AMP even upon addition of nucleotides in excess. However, the [**V4**–Pyr] complex responded towards AMP, albeit at higher concentrations (10^{-2} M). In HEPES buffer (pH = 7.4), the CT aggregates of [**V1**–Pyr] and [**V2**–Pyr] dissolved completely; still they responded to AMP with enhancement in emission intensity (Fig. S31a and b, ESI†). In order to acquire deeper insight into the interaction between the [**V1**–Pyr] or [**V2**–Pyr] aggregates and the nucleotides, absorption spectra of the CT suspensions were evaluated upon addition of nucleotides. Akin to the emission spectra, their absorption spectra did not reveal any change with ATP and ADP. In the presence of AMP, concomitant with disaggregation, Mie scattering disappeared from the absorption spectra of [**V1**–Pyr] or [**V2**–Pyr] suspensions with evolution of a new feature at 456 nm, characteristic of the deprotonated form of pyranine (*cf.* Fig. S31c, ESI†).

Based on the above results, we conclude that [**V1**–Pyr] and [**V2**–Pyr] suspensions are capable of serving as fluorogenic AMP sensors. Sodium salts of AMP were basic enough to deprotonate the protons of carboxylic acid moieties and pyranine resulting in disruption of H-bonding and emission enhancement that led to dissolution of aggregates. This approach provides an alternate avenue towards sensing nucleotides *via* a naked-eye detection module that allows sensing of AMP with the transition of a suspension to a true solution. The above results were quite surprising given the nature of interactions reported between the viologen–pyranine CT complexes and the nucleotides, which were driven *via* electrostatic and π–π stacking interactions. Literature reports[59] on nucleotide sensing stem from a combination of electrostatic interactions, π–π stacking and host–guest interactions. However, the recognition here is due to disruption of hydrogen bonding leading to disaggregation, which resulted in a clear solution. To the best of our knowledge such reports do not exist for AMP recognition. It is noteworthy here to mention that, this approach suffers from strong interference from basic anions. Optimizing the nature of substituents on viologen, pH and other variables could lead to a robust nucleotide recognition system.

Summary

Alkyl and alkyl carboxylic acid derivatized viologens (**V1** to **V5**) were synthesized and characterized by appropriate spectroscopic techniques. **V1** to **V4** exhibited excellent solubility in water while **V5** was insoluble. Upon CT interaction of **V1** to **V4** with pyranine in water, (i) an instantaneous aggregation accompanied by colour change in the case of **V1** and **V2** and (ii) color change without aggregation in the case of **V3** and **V4** were observed. The fundamental driving forces towards supramolecular assembly of [**V1**–Pyr] and [**V2**–Pyr] CT complexes in water were a combination of charge transfer, coulombic, hydrophobic and hydrogen bonding interactions. The adopted design for the viologens enabled the latter two interactions to synergistically complement each other resulting in the generation of geometrically specific supramolecular aggregates. Absence of either of them did not bring about aggregation. While cuboidal shaped supramolecular aggregates were observed in the case of the [**V1**–Pyr] CT complex, the [**V2**–Pyr] assembly revealed co-existence of cuboidal aggregates dispersed over a fibrous matrix. These aggregates in aqueous solution exhibited reversible response towards variation in pH. Ultimately, the CT aggregates of [**V1**–Pyr] and [**V2**–Pyr] exhibited selective response towards adenosine monophosphate by deprotonation induced dissolution of aggregates in water, leading to an increase in emission enhancement.

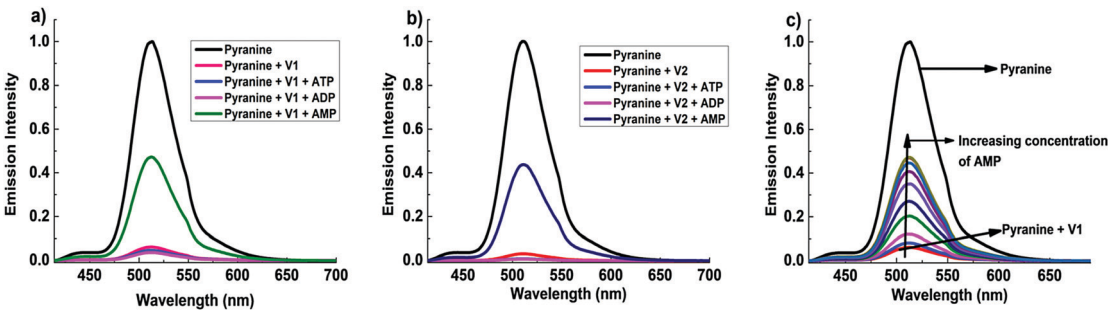

Fig. 10 (a and b) Emission response of **V1**–pyranine and **V2**–pyranine suspensions towards adenosine nucleotides in water; (c) emission response of the [**V1**–Pyr] suspension towards AMP in water.

Conclusions

In conclusion, we developed an environmentally benign approach towards developing water insoluble and pH responsive cuboidal and tubular supramolecular aggregates from water soluble precursors. Aggregates were stable enough to be isolated through filtration. Such stimuli-responsive aggregates hold promise towards development of pH controlled drug release systems. This green approach towards generating solvent processable supramolecular polymers also provides ample scope to develop micro- and nanoscale structures for diverse applications. By varying the nature of groups attached to the nitrogen atoms of bipyridine, such as the length of the alkyl chain and the alkyl carboxylic acids, introducing branching and fluorination in the alkyl chains, and varying the nature of counter anions, solvent, *etc.*, fine tunable aggregates of diverse properties can be designed and fabricated for futuristic applications.

Conflicts of interest

There are no conflicts to declare.

Acknowledgements

Redhills L. Narendran thanks the University Grants Commission of India for fellowship. IIT Madras is thankfully acknowledged for the infrastructural facilities.

References

1 J.-M. Lehn, *Supramolecular Chemistry: Concepts and Perspectives*, Wiley-VCH, Weinheim, 1995.
2 J.-M. Lehn, *Proc. Natl. Acad. Sci. U. S. A.*, 2002, **99**, 4763.
3 F. Gutmann, C. Johnson, H. Keyzer and J. Molnar, *Charge Transfer Complexes in Biochemistry Systems*, Marcel Dekker, New York, 1997.
4 J. Brédas, D. Beljonne, V. Coropceanu and J. Cornil, *Chem. Rev.*, 2004, **104**, 4971.
5 F. J. M. Hoeben, P. Jonkheijm, E. W. Meijer and A. P. H. J. Schenning, *Chem. Rev.*, 2005, **105**, 1491.
6 V. Balzani, A. Credi and M. Venturi, *Molecular Devices and Machines: Concepts and Perspectives for the Nanoworld*, Wiley-VCH, Weinheim, 2008.
7 S. Erbas-Cakmak, D. A. Leigh, C. T. McTernan and A. L. Nussbaumer, *Chem. Rev.*, 2015, **115**, 10081.
8 S. G. Ramkumar and S. Ramakrishnan, *Macromolecules*, 2010, **43**, 2307.
9 M. Pandeeswar, S. P. Senanayak, K. S. Narayan and T. Govindaraju, *J. Am. Chem. Soc.*, 2016, **138**, 8259.
10 P. H. J. Kouwer, W. F. Jager, W. J. Mijs and S. J. Picken, *Macromolecules*, 2002, **35**, 4322.
11 C. Wang, Z. Wang and X. Zhang, *Acc. Chem. Res.*, 2012, **45**, 608.
12 J. Raeburn and D. J. Adams, *Chem. Commun.*, 2015, **51**, 5170.
13 J. N. Israelachvilli, *Intermolecular and Surface Forces*, Academic Press, 3rd edn, 2011.
14 S. Yagai, S. Okamura, Y. Nakano, M. Yamauchi, K. Kishikawa, T. Karatsu, A. Kitamura, A. Ueno, D. Kuzuhara, H. Yamada, T. Seki and H. Ito, *Nat. Commun.*, 2014, **5**, 4013.
15 M. Voggel, R. M. Meinusch, V. Siewert, M. Kunkel, V. Wittmann and S. Polarz, *Soft Matter*, 2018, **14**, 7214.
16 R. Nagarajan, *Langmuir*, 2002, **18**, 31.
17 C. Wang, S. Yin, S. Chen, H. Xu, Z. Wang and X. Zhang, *Angew. Chem., Int. Ed.*, 2008, **47**, 9049.
18 D. Jia, J. Geng, X. J. Loh, D. Das, T.-C. Lee and O. A. Scherman, *Angew. Chem., Int. Ed.*, 2012, **51**, 9633.
19 L. Striepe and T. Baumgartner, *Chem. – Eur. J.*, 2017, **23**, 16924.
20 A. F. Greene, M. K. Danielson, A. O. Delawder, K. P. Liles, X. Li, A. Natraj, A. Wellen and J. C. Barnes, *Chem. Mater.*, 2017, **29**, 9498.
21 C. Wang, Y. Guo, Z. Wang and X. Zhang, *Langmuir*, 2010, **26**, 14509.
22 W. Yu, X.-Y. Wang, J. Li, Z.-T. Li, Y.-K. Yan, W. Wang and J. A. Pei, *Chem. Commun.*, 2013, **49**, 54.
23 Y.-D. Huang, P. Huo, M.-Y. Shao, J.-X. Yin, W.-C. Shen, Q.-Y. Zhu and J. Dai, *Inorg. Chem.*, 2014, **53**, 3480.
24 G. J. Moody, R. K. Owusu, A. M. Z. Slawin, N. Spencer, J. F. Stoddart, R. J. D. Thomas and D. J. Williams, *Angew. Chem., Int. Ed. Engl.*, 1987, **26**, 890.
25 H. Yao and T. Enseki, *Langmuir*, 2017, **33**, 219.
26 R. Tanaka, A. Okazawa, H. Konaka, A. Sasaki, N. Kojima and N. Matsushita, *Inorg. Chem.*, 2018, **57**, 2209.
27 T. Yuan, Y. Xu, C. Zhu, Z. Jiang, H.-J. Sue, L. Fang and M. A. Olson, *Chem. Mater.*, 2017, **29**, 9937.
28 A. N. Swinburne, M. J. Paterson, K. H. Fischer, S. J. Dickson, E. V. B. Wallace, W. J. Belcher, A. Beeby and J. W. Steed, *Chem. – Eur. J.*, 2010, **16**, 1480.
29 P. P. Neelakandan, M. Hariharan and D. Ramaiah, *Org. Lett.*, 2005, **7**, 5765.
30 E. G. Hvastkovs and D. A. Buttry, *Langmuir*, 2006, **22**, 10821.
31 E. B. de Borba, C. L. C. Amaral, M. J. Politi, R. Villalobos and M. S. Baptista, *Langmuir*, 2000, **16**, 5900.
32 D. B. Cordes, S. Gamsey, Z. Sharrett, A. Miller, P. Thoniyot, R. A. Wessling and B. Singaram, *Langmuir*, 2005, **21**, 6540.
33 S. Gamsey, A. Miller, M. M. Olmstead, C. M. Beavers, L. C. Hirayama, S. Pradhan, R. A. Wessling and B. Singaram, *J. Am. Chem. Soc.*, 2007, **129**, 1278.
34 P. P. Neelakandan, M. Hariharan and D. A. Ramaiah, *J. Am. Chem. Soc.*, 2006, **128**, 11334.
35 M. Schäferling, T. Lang and A. Schnettelker, *J. Lumin.*, 2014, **154**, 458.
36 K. Liu, Y. Yao, Y. Liu, C. Wang, Z. Li and X. Zhang, *Langmuir*, 2012, **28**, 10697.
37 K. Liu, Y. Yao, C. Wang, Y. Liu, Z. Li and X. Zhang, *Chem. – Eur. J.*, 2012, **18**, 8622.
38 K. Jalani, S. Dhiman, A. Jain and S. J. George, *Chem. Sci.*, 2017, **8**, 6030.
39 C. Wang, Y. Guo, Y. Wang, H. Xu, R. Wang and X. Zhang, *Angew. Chem., Int. Ed.*, 2009, **48**, 8962.
40 S. Datta, N. Dey and S. Bhattacharya, *Chem. Commun.*, 2017, **53**, 2371.

41 G. A. Jeffrey and A. Saenger, *Hydrogen Bonding in Biological Structures*, Springer-Verlag, New York, Heidelberg, 1991.
42 G. Armstrong and M. Buggy, *J. Mater. Sci.*, 2005, **40**, 547.
43 E. D. Glowacki, M. Irimai-Vladu, S. Bauer and N. S. Sariciftci, *J. Mater. Chem. B*, 2013, **1**, 3742.
44 C. M. A. Leenders, M. B. Baker, I. A. B. Pijpers, R. P. M. Lafleur, L. Albertazzi, A. R. A. Palmans and E. W. Meijer, *Soft Matter*, 2016, **12**, 2887.
45 C. M. A. Leenders, L. Albertazzi, T. Mes, M. M. E. Koenigs, A. R. A. Palmans and E. W. Meijer, *Chem. Commun.*, 2013, **49**, 1963.
46 E. Obert, M. Bellot, L. Bouteiller, F. Andrioletti, C. L. Ferrenbach and F. Boue, *J. Am. Chem. Soc.*, 2007, **129**, 15601.
47 B.-K. An, S.-K. Kwon, S.-D. Jung and S. Y. Park, *J. Am. Chem. Soc.*, 2002, **124**, 14410.
48 H. Auweter, H. Haberkorn, W. Heckmann, D. Horn, E. Lüddecke, J. Rieger and H. Weiss, *Angew. Chem., Int. Ed.*, 1999, **38**, 2188.
49 M. Bass, E. W. V. Stryland, D. R. Williams and W. L. Wolfe, *Handbook of Optics*, McGraw-Hill, New York, 1995.
50 S. E. A. Gratton, P. A. Ropp, P. D. Pohlhaus, J. C. Luft, V. J. Madden, M. E. Napier and J. M. Desimone, *Proc. Natl. Acad. Sci. U. S. A.*, 2008, **105**, 11613.
51 W. Zhang and C. Gao, *J. Mater. Chem. A*, 2017, **5**, 16059.
52 M. S. Bakshi, *Cryst. Growth Des.*, 2016, **16**, 1104.
53 Z. Liang, A. Susha and F. Caruso, *Chem. Mater.*, 2003, **15**, 3183.
54 M. Kumar, K. V. Rao and S. J. George, *Phys. Chem. Chem. Phys.*, 2014, **16**, 1300.
55 Y. He, J. Xu, X. Sun, X. Ren, A. Maharjan, P. York, Y. Su, H. Li and J. Zhang, *Theranostics*, 2019, **9**, 2489.
56 J. F. Alexander, V. Kozlovskaya, J. Chen, T. Kuncewicz, E. Kharlampieva and B. Godin, *Adv. Healthcare Mater.*, 2015, **4**, 2657.
57 C. R. Martinez and B. L. Iverson, *Chem. Sci.*, 2012, **3**, 2191.
58 B. A. Ikkanda and B. L. Iverson, *Chem. Commun.*, 2016, **52**, 7752.
59 A. M. Agafontsev, A. Ravi, T. A. Shumilova, A. S. Oshchepkov and E. A. Kataev, *Chem. – Eur. J.*, 2019, **25**, 2684.

